


Boosting entanglement growth of many-body localization by superpositions of disorderJhen-Dong Lin* and Yueh-Nan Chen[†]*Department of Physics, National Cheng Kung University, 701 Tainan, Taiwan
and Center for Quantum Frontiers of Research & Technology, NCKU, 70101 Tainan, Taiwan* (Received 18 April 2023; accepted 12 July 2023; published 7 August 2023)

Many-body localization (MBL) can occur when strong disorders prevent an interacting system from thermalization. To study the dynamics of such systems, performing an ensemble average over many different disorder configurations is typically necessary. Previous works have utilized an algorithm in which different disorder profiles are mapped into a quantum ancilla. By preparing the ancilla in a quantum superposition state, quantum parallelism can be harnessed to obtain the ensemble average in a single computation run. In this work, we modify this algorithm by performing a measurement on the ancilla. This enables the determination of conditional dynamics not only by the ensemble average but also by the quantum interference effect. Using a phenomenological analysis based on local integrals of motion, we demonstrate that this protocol can lead to an enhancement of the dephasing effect and a boost in entanglement growth for systems in the deep MBL phase. For a typical MBL system with short-range interactions, reaching saturation in entanglement usually takes an exponentially long time, which makes experimental explorations of long-time properties challenging. With our protocol, we demonstrate a significant reduction in the saturation time by several orders. This advancement facilitates easier access to the behavior in the long-time regime. We also present numerical simulations of the random XXZ model where this enhancement is also present in a smaller disorder strength, beyond the deep MBL regime.

DOI: [10.1103/PhysRevA.108.022203](https://doi.org/10.1103/PhysRevA.108.022203)**I. INTRODUCTION**

Thermalization is ubiquitous in nonintegrable many-body systems. However, in a seminal work [1], Anderson demonstrated that strong disorder can restore the integrability and prevent the thermalization of noninteracting systems, a phenomenon termed Anderson localization. Recently, both experimental and theoretical investigations have shown that strong disorders can also localize interacting systems, which is known as many-body localization (MBL) [2–4]. One of the milestones in this field is the proposal of a phenomenological model called local integrals of motions (LIOMs) [5–11], which characterizes MBL systems with extensive conserved quantities. From the perspective of LIOMs, the slow logarithmic entanglement growth [12–14]—the hallmark of MBL—can be explained by the dephasing mechanism together with the exponential decay law for interactions among LIOMs. This insight has led to experimental proposals such as spin-echo-type experiments [15–17] to identify MBL systems.

To extract meaningful information from such random disordered systems, an ensemble average over many disorder configurations is usually necessary, which could be a resource-intensive task. In Ref. [18], the authors proposed an algorithm that utilizes quantum parallelism to address this issue. The main idea is to encode different disorder profiles into a quantum ancilla. The ancilla can be prepared in a quantum

superposition state, allowing the MBL dynamics for different profiles to run in parallel. By tracing out the ancilla at the end, the ensemble average results can be obtained in a single computation or experiment run [19–21].

Recently, the idea of using quantum ancilla to evolve systems in parallel has also been adopted in various applications, including communication channels [22–27], quantum thermodynamics [28–31], quantum metrology [32–34], open quantum systems [35–38], and relativistic quantum theory [39–41]. However, instead of directly discarding the ancilla after an evolution, these works considered performing a measurement on the ancilla. In this case, the conditional state of the system may depend not only on the ensemble average but also on the quantum interference effect among different quantum evolutions, leading to nontrivial results.

Motivated by these works, we modify the algorithm proposed in Ref. [18] by performing an additional measurement, as mentioned earlier. Our aim is to investigate the potential impacts of this modified algorithm on MBL systems. Here, we focus on spin-chain systems with on-site disorder together with short-range interactions. We first provide analytical and numerical analysis based on LIOM representation. Our findings show that the quantum interference for different evolutions (disorder profiles) can generally enhance the dephasing effect and boost the entanglement growth for systems in the deep MBL phase. As aforementioned, MBL systems usually demonstrate slow logarithmic entanglement growth, implying that the associated saturation times could be exponentially large. Consequently, exploring long-time behavior experimentally presents a formidable challenge. By utilizing

*jhendonglin@gmail.com

†yuehnan@mail.ncku.edu.tw

our protocol, we show that the saturation time can be significantly reduced by several orders, making the behavior in the long-time regime much more accessible.

Moreover, we consider the random XXZ model [12,42,43], the well-investigated model in the context of MBL, with parameters ranging from small to strong disorder strengths. We also consider the case that can manifest Anderson localization. The numerical results demonstrate a significant enhancement of entanglement growth, while retaining the system's initial memory in both the scenarios of many-body localization and Anderson localization. The results also indicate that superpositions of disorders can reduce the saturation time to an experimentally achievable regime. Furthermore, the protocol can lead to a faster increase when the system size increases, suggesting that the volume law of entanglement [13,14] could be more visible in experiments.

The rest of this paper is organized as follows. In Sec. II, we formulate the algorithm and present a phenomenological analysis based on the LIOM representation. In Sec. III, we present numerical results for the random XXZ model that can demonstrate either many-body or Anderson localization. Finally, we draw our conclusion in Sec. IV.

II. PHENOMENOLOGICAL ANALYSIS

Throughout this work, we focus on one-dimensional spin chains with on-site disorder and short-range interactions, e.g., the random XXZ model that is discussed later. In this section, we keep the Hamiltonian of the system unspecified and consider the well-known phenomenological model for MBL. Specifically, when the spin chain is in an MBL phase, there exist extensively conserved quantities that can be obtained by the quasilocal unitary transformation U such that

$$\begin{aligned} \tau_{z,i} &= U^\dagger \sigma_{z,i} U \\ &= \sigma_{z,i} + \sum_{j,k} \sum_{\alpha,\beta=x,y,z} C_{\alpha,\beta}(j,k) \sigma_{\alpha,j} \sigma_{\beta,k} + \dots \end{aligned} \quad (1)$$

Here, $\{\sigma_{\alpha,i}\}_{\alpha=x,y,z}$ are the usual Pauli operators on site i , and $\tau_{z,i}$ is the conserved quantity associated with $\sigma_{z,i}$. The coefficient $C_{\alpha,\beta}(j,k)$ decays exponentially with the distance between the spins j and k . Conventionally, $\tau_{z,i}$ and $\sigma_{z,i}$ are called the localized bit (l-bit) and the physical bit (p-bit), respectively. In other words, l-bits can be regarded as p-bits associated with quasilocal dressings. Because these l-bits are conserved, the diagonalized system's Hamiltonian can be written, in general, as

$$H_{\text{MBL}} = \sum_i h_i \tau_{z,i} + \sum_{i<j} J_{i,j} \tau_{z,i} \tau_{z,j} + \dots \quad (2)$$

Here, h_i denotes the on-site potential and $J_{i,j}$ represents the interaction between these l-bits, which is described by an exponential decay law, i.e., $J_{i,j} = \tilde{J}_{i,j} \exp(-|i-j|/\xi)$. Here, ξ denotes a dimensionless characteristic length. Note that the parameters h_i , $\tilde{J}_{i,j}$, and $C_{\alpha,\beta}(j,k)$ depend on the specific realization of the on-site potential for the spin chain under investigation. Since the on-site potential is usually characterized by a random variable, we expect that these parameters should also inherit the randomness.

This model captures several dynamical features of a generic MBL system. For instance, the characteristic trait of slow entanglement generation can be described by the dephasing interactions among these l-bits. Specifically, due to the exponential decay of the interaction between two distant l-bits, it takes an exponentially long time to build up entanglement, which results in a logarithmic entanglement growth [16,17]. As an example, we consider an initial product state:

$$|\psi_0\rangle = \frac{1}{\sqrt{2}}(|\uparrow\rangle + |\downarrow\rangle) \otimes \frac{1}{\sqrt{2}}(|\uparrow\rangle + |\downarrow\rangle) \otimes \dots, \quad (3)$$

where $\tau_z|\uparrow\rangle = |\uparrow\rangle$ and $\tau_z|\downarrow\rangle = -|\downarrow\rangle$. We focus on the reduced dynamics of the first l-bit (i.e., $j = 1$). Additionally, we consider a simplified variant of the model Hamiltonian where we only keep the two-body interactions in Eq. (2):

$$\begin{aligned} \tilde{H}_{\text{MBL}} &= \sum_{i<j} J_{i,j} \tau_{z,i} \tau_{z,j} \\ &= |\uparrow_1\rangle\langle\uparrow_1| \sum_{j>1} J_{1,j} \tau_{z,j} - |\downarrow_1\rangle\langle\downarrow_1| \sum_{j>1} J_{1,j} \tau_{z,j} + H', \end{aligned} \quad (4)$$

with $H' = \sum_{1<i<j} J_{i,j} \tau_{z,i} \tau_{z,j}$.

In this case, the reduced dynamics of the first l-bit can be expressed as

$$\begin{aligned} \rho(t) &= \text{tr}_{j>1} [\exp(-i\tilde{H}_{\text{MBL}}t) |\psi_0\rangle\langle\psi_0| \exp(i\tilde{H}_{\text{MBL}}t)] \\ &= \frac{1}{2} [|\uparrow\rangle\langle\uparrow| + |\downarrow\rangle\langle\downarrow| + \phi(t) |\uparrow\rangle\langle\downarrow| + \phi(t)^* |\downarrow\rangle\langle\uparrow|], \end{aligned} \quad (5)$$

where the dephasing factor is given by

$$\phi(t) = \prod_{j>1} \cos(2J_{1,j}t). \quad (6)$$

The dephasing factor directly reflects the entanglement dynamics. For instance, one can quantify the entanglement between the first and other l-bits by linear entanglement entropy, i.e., $S_L = (1 - |\phi(t)|^2)/2$.

Here, we consider that the prefactor $\tilde{J}_{i,j}$ is uniformly drawn from the interval $[-\mathcal{J}, \mathcal{J}]$, suggesting that the dynamics can be divided into two regimes according to the product form in Eq. (6). (i) The short-time regime where $\mathcal{J}t \leq \exp(1/\xi)$ and the entanglement generation are governed by the interactions nearby the first l-bit (i.e., $|1-j| < \xi$), resulting in a power-law increase in the entanglement entropy. (ii) When $\mathcal{J}t \gg \exp(1/\xi)$, the dynamics is governed by the long-range interactions (i.e., $|1-j| > \xi$), where the effect of the exponential decay factor in the interactions becomes significant and results in the logarithmic entanglement growth. Note that $\phi(t)$ is independent of the evolution governed by H' , wherein the interactions do not involve the first l-bit. However, as shown in the following, this is not the case when we consider quantum superpositions of disorders by using the quantum ancilla, which leads to faster entanglement growth.

Let us consider our algorithm, bearing in mind that the explicit expressions of $\tau_{z,i}$ and the diagonalized Hamiltonian described by Eq. (2) depend on the specific parameters of the system, such as a particular disorder configuration. However, in a deep MBL regime, e.g., the strong disorder limit, the dressing terms in Eq. (1) become negligible [i.e.,

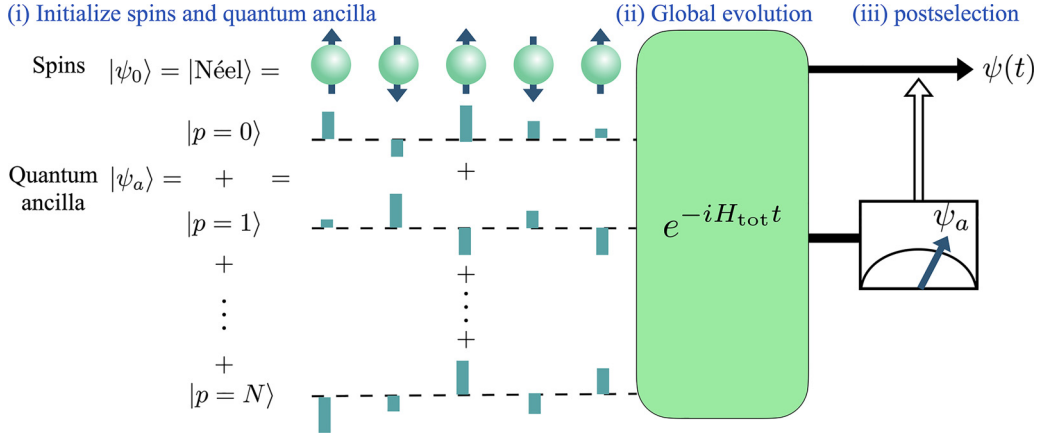


FIG. 1. Schematic illustration of the algorithm for a spin chain subject to a “quantum superposition” of random on-site potential (presented by the histograms), where the profiles are encoded in a quantum ancilla. In step (i), we prepare the ancilla in a quantum superposition state $|\psi_a\rangle = \sum_p |p_a\rangle / \sqrt{N}$, that is, the superposition of profiles of on-site potentials. In step (ii), the total system is evolved according to the Hamiltonian defined in Eq. (7) to achieve quantum parallel computation. In step (iii), we postselect the spin system associated with the ancilla state $|\psi_a\rangle$, and the conditional state of the spin $|\psi(t)\rangle$ can be obtained.

$C_{\alpha,\beta}(j, k) \approx 0$] and the l-bits and p-bits roughly coincide. Along this reasoning, we expect that different disorder profiles will give rise to different realizations of the prefactors $\{\tilde{J}_{i,j}\}$ of the diagonalized Hamiltonian, while the explicit expressions of l-bits remain unchanged.

Suppose we encode N different disorder profiles into a quantum ancilla, which can then determine N different evolutions. The ancilla-system total Hamiltonian is given by

$$H_{\text{tot}} = \sum_{p=1}^N |p_a\rangle\langle p_a| \otimes \tilde{H}_{\text{MBL}}(\{J_{i,j}^{(p)}\}). \quad (7)$$

Here, $\tilde{H}_{\text{MBL}}(\{J_{i,j}^{(p)}\})$ denotes the Hamiltonian with a specified realization of the interactions $\{J_{i,j}^{(p)}\}$, and $\{|p_a\rangle\}$ forms an orthonormal basis with $\langle p_a|p'_a\rangle = \delta_{p,p'}$. In Fig. 1, we illustrate the algorithm for a spin chain subject to on-site random potentials, which can be divided into three steps.

(i) Initialization. We initialize the spin system in state $|\psi_0\rangle$. In this section, we consider the state in Eq. (3). In Sec. III, we consider the Néel state, which is formally introduced later. The quantum ancilla is prepared in a superposition state $|\psi_a\rangle = \sum_p |p_a\rangle / \sqrt{N}$ to achieve quantum superposition of disorder configurations.

(ii) Global evolution. We let the ancilla-spin system evolve. The time-dependent state can then be written as

$$|\psi_{\text{tot}}(t)\rangle = \frac{1}{\sqrt{N}} \sum_p |p_a\rangle \otimes \exp[-i\tilde{H}_{\text{MBL}}(\{J_{i,j}^{(p)}\})t] |\psi_0\rangle. \quad (8)$$

(iii) Postselection. We postselect the state $|\psi_a\rangle$ on the ancilla before discarding it. After the postselection, the conditional state of the system reads

$$|\psi(t)\rangle = \frac{|\tilde{\psi}(t)\rangle}{\|\tilde{\psi}(t)\|},$$

with $|\tilde{\psi}(t)\rangle = \frac{1}{N} \sum_p \exp[-i\tilde{H}_{\text{MBL}}(\{J_{i,j}^{(p)}\})t] |\psi_0\rangle. \quad (9)$

The effective dephasing factor of the first l-bit can be described by

$$\phi_{\text{eff}}(t) \propto \frac{1}{N^2} \sum_{p,q} \langle \psi'_0 | \hat{F}_{p,q}(t) \hat{G}_{p,q}(t) | \psi'_0 \rangle,$$

with

$$\hat{F}_{p,q}(t) = \exp(-i[H^{(p)} - H^{(q)}]t),$$

$$\hat{G}_{p,q}(t) = \exp\left[-i \sum_{j>1} (J_{1,j}^{(p)} + J_{1,j}^{(q)}) \tau_{z,j} t\right],$$

$$|\psi'_0\rangle = \bigotimes_{j>1} \frac{|\uparrow_j\rangle + |\downarrow_j\rangle}{\sqrt{2}}. \quad (10)$$

Note that the effective dephasing factor now includes the term H' through the factor $\hat{F}_{p,q}(t)$, with $p \neq q$, which originates from the quantum interference effect [38] between the profiles p and q . This factor introduces additional contributions of interactions, i.e., $J_{i,j}$ with $i, j > 1$, into the dephasing factor. Following the intuition of the product form in Eq. (6), one can expect that the dephasing effect and the entanglement growth will become stronger. To confirm this intuition, in Fig. 2, we

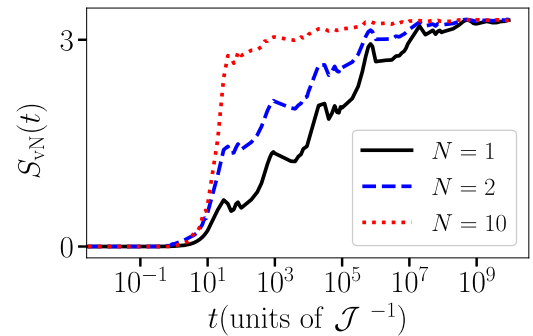


FIG. 2. Time evolutions of half-chain entanglement of an eight-l-bit system with 1, 2, and 10 superposed disorder configurations. Here $\mathcal{J} = 1$ and $\xi = 0.3$. The results are averaged over 1000 disorder realizations.

present numerical simulations of entanglement dynamics for an eight-1-bit system with $\mathcal{J} = 1$ and $\xi = 0.3$. The entanglement is quantified by the half-chain von Neumann entropy $S_{vN} = -\text{tr} \rho \log_2 \rho$, where ρ denotes the half-chain reduced density matrix. One can clearly observe that entanglement growth is enhanced as the number of superposed evolutions N increases. Therefore, the results indicate that *the quantum interference effect for dynamics with different disorder profiles can enhance the entanglement growth for a generic system in the deep MBL regime*. Moreover, we can observe that the saturation time of entanglement significantly decreases by several orders. More specifically, the saturation times for the cases of $N = 1$, $N = 2$, and $N = 10$ are roughly of the orders 10^9 , 10^7 , and 10^5 in units of $1/\mathcal{J}$. In practice, this could make the investigations of long-time properties much more accessible.

III. XXZ CHAIN WITH RANDOM EXTERNAL FIELD

In this section, we consider an XXZ Heisenberg chain with a random external field [12,42,43], where the Hamiltonian reads

$$H_{XXZ} = \sum_i g(S_{x,i}S_{x,i+1} + S_{y,i}S_{y,i+1}) + \Delta S_{z,i}S_{z,i+1} + \sum_i h_i S_{z,i}. \quad (11)$$

Here, $\{S_{x,i} = \sigma_{x,i}/2, S_{y,i} = \sigma_{y,i}/2, S_{z,i} = \sigma_{z,i}/2\}$ denote spin-1/2 operators on site i . Also, g and Δ describe the hopping and interaction energies between each spin and their nearest neighbors. The h_i represents the strength of the external field on site i and is uniformly drawn from $[-W, W]$, with W being the disorder strength. When the disorder strength is sufficiently strong, the system can display localization behavior. Note that, for the case $\Delta = 0$, the system can exhibit Anderson localization, whereas for the case $\Delta \neq 0$, the system can demonstrate many-body localization. In addition to the entanglement dynamics, we also consider the imbalance, which is an experimental relevant quantifier of the system's memory [44–49], as an indicator for the localization behavior. We initialize the system in the Néel state, i.e.,

$$|\psi_{\text{Néel}}\rangle = |1, -1, 1, -1, \dots\rangle, \quad (12)$$

with $\sigma_z|\pm 1\rangle = \pm|\pm 1\rangle$. The imbalance is defined as

$$I(t) = \sum_{i=1} (-1)^{i+1} \langle \psi(t) | \sigma_{z,i} | \psi(t) \rangle. \quad (13)$$

Since the imbalance quantifies the amount of the initial memory of the system at the time t , one expects that the $I(t)$ decays to zero in an ergodic (thermalized), implying that the initial memory is completely lost. Therefore, the presence of a nonzero value of imbalance in the long-time limit suggests that the system is in a localized phase.

In Fig. 3, we present the dynamics of the half-chain entanglement S_{vN} and the imbalance $I(t)$ for an eight-spin chain with different numbers of superposed disorder profiles N . Throughout the following discussions, we set the hopping energy $g = 1$. We consider both the cases $\Delta = 0.2$ and $\Delta = 0$ and set $W = 3$ so that many-body localization and Anderson localization can be observed. As shown in Fig. 3(a), for the

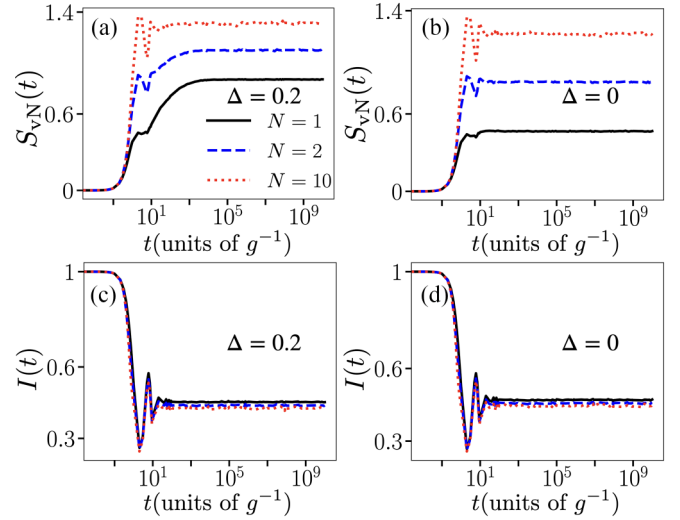


FIG. 3. Time evolutions of entanglement entropy [panels (a) and (b)] and imbalance [panels (c) and (d)] for different numbers of profiles N in quantum superposition. The disorder strength is $W = 3$, and we consider $\Delta = 0.2$ and $\Delta = 0$, which can demonstrate many-body localization and Anderson localization, respectively. The results are obtained by averaging over 10 000 disorder realizations.

case of $\Delta = 0.2$, one can observe a slow logarithmic growth in S_{vN} followed by an initial fast growth, which is the hallmark of many-body localization. In contrast, for the case of $\Delta = 0$ [Fig. 3(b)], i.e., Anderson localization, the slow logarithmic growth is absent. One can also observe that increasing the number N can boost the initial entanglement growth and enhance the saturated entanglement for both cases. Furthermore, for the case $\Delta = 0.2$, the duration for the logarithmic growth becomes shorter when increasing the number N . However, the enhancement of entanglement does not imply a strong thermalization of the system, as shown in Figs. 3(c) and 3(d), where we find that the dynamics and the saturation value of the imbalance $I(t)$ are relatively insensitive to the number N , suggesting that the system can stay in a localized phase. In other words, the initial memory can be preserved, while generating more entanglement among the spins. Therefore, one can conclude that increasing the number N results in a stronger dephasing effect, as suggested in the previous section.

In Figs. 4(a)–4(d), we present the saturation values of S_{vN} and I with different disorder strengths $W = \{1, 3, 5\}$. The saturation values are defined by

$$Q_{\text{sat}} = \frac{1}{t_f - t_i} \int_{t_i}^{t_f} dt Q(t), \quad (14)$$

with $Q \in \{S_{vN}, I\}$. Also, we set $t_i/g = 10^9$ and $t_f/g = 10^{10}$. In Fig. 4(e), we consider the saturation time of S_{vN} (for the case $\Delta = 0.2$), which is defined by

$$T_{\text{sat}} = \min t \text{ such that } |S_{vN}(t) - S_{vN,\text{sat}}| < \epsilon. \quad (15)$$

Here, we set the tolerance $\epsilon = 10^{-3}$. One can observe that, when W decreases, I_{sat} ($S_{vN,\text{sat}}$) decreases (increases), indicating that the system becomes more thermalized as the disorder strength decreases. Further, for a fixed W , one can observe

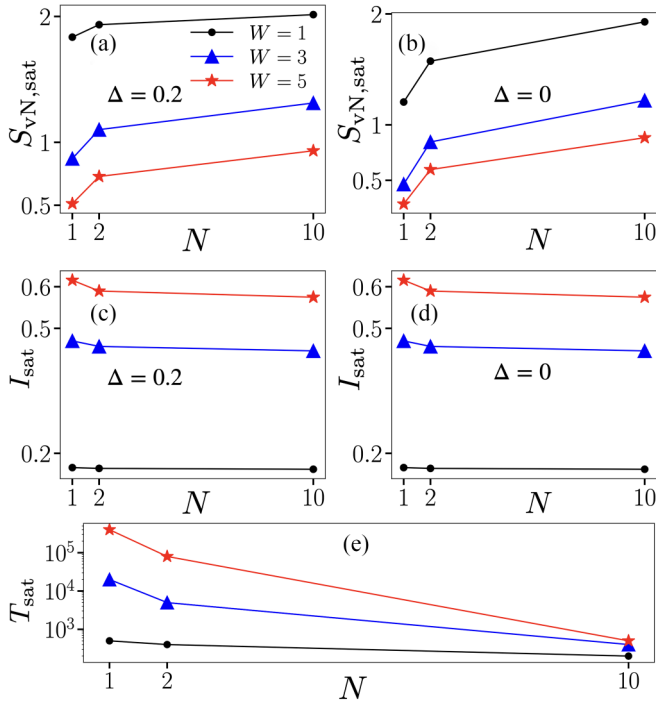


FIG. 4. (a)–(d) The saturation values of entanglement entropy and imbalance for different disorder strengths and different numbers of superposed profiles. The many-body localization scenario ($\Delta = 0.2$) and the Anderson localization scenario ($\Delta = 0$) are considered. (e) The saturation time (for the case $\Delta = 0.2$) of the entanglement entropy for different disorder strengths and different numbers of superposed profiles. All of the results are obtained by averaging over 10 000 disorder realizations.

that $S_{vN,sat}$ is enhanced when N increases. In addition, we can find that increasing N does not significantly reduce I_{sat} even for a smaller disorder strength. It means that the mechanism, enhancing the dephasing effect, also manifests beyond the deep MBL regime for this model. We can also observe that the saturation time of entanglement T_{sat} significantly reduces for a larger disorder strength. In particular, for the case of $N = 10$, the saturation time can be reduced to roughly thousands of tunneling time ($T_{sat}/g \approx 10^3$) that could be achievable for current experiments [44–47].

Finally, we investigate the volume law of entanglement by considering $S_{vN,sat}$ for different sizes of spin chains as shown in Fig. 5. The number of spins ranges from 6 to 12. For the ordinary ensemble average results (i.e., $N = 1$), the saturated entanglement for $\Delta = 0.2$ ($\Delta = 0$) demonstrates a volume (area) law. This means that $S_{vN,sat}$ increases (remains constant) as the length of the spin chain increases [16,17]. In addition, when considering a larger number N of superposed profiles, we can observe that the saturated entanglement displays a more rapid growth relative to the system size. This phenomenon could enhance the visibility of the volume-law signal for both experimental and theoretical investigations. Note that both the value of saturated entanglement and the rate of increase with respect to system size are higher for the case of $\Delta = 0.2$ compared to that of $\Delta = 0$. This obser-

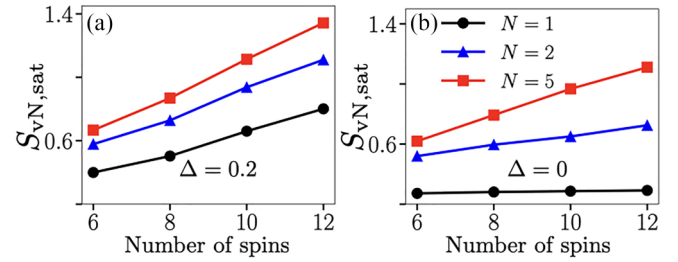


FIG. 5. The saturation values of entanglement entropy for different numbers of superposed profiles with respect to different lengths of the spin chain. The disorder strength is $W = 5$, and the results are obtained by averaging over 1000 disorder realizations.

vation aligns with the physical intuition that the interaction terms can lead to a stronger generation of entanglement.

IV. CONCLUSIONS

We consider an algorithm which can superpose dynamics with different disorder profiles, and we investigate its impact on MBL systems. Through a phenomenological analysis, we demonstrate that the interference effect can result in an enhancement of entanglement generation for spin-chain systems in a deep MBL regime. Moreover, we present numerical simulations on the random XXZ model and consider two scenarios that can manifest many-body localization and Anderson localization. For both cases, the long-time saturated entanglement is enhanced. Notably, the protocol can significantly reduce the saturation time and enhance the volume-law behavior of entanglement for the MBL scenario. This makes the long-time properties more visible and easier to explore.

This work raises several open questions. For instance, a direct extension of this work is to consider long-range interaction [50–54], which is a built-in feature for various physical systems. Also, since our protocol can be used to manipulate the entanglement properties of MBL systems, it is natural to ask about its implications for practical applications, e.g., quantum many-body battery [55] and quantum computation [56], etc. From a more general perspective, the proposed algorithm can be regarded as a many-body engineering protocol. Therefore, it would be intriguing to investigate its applications to other exotic many-body effects, such as quantum information scrambling [57–61] and quantum time crystals [62].

Regarding the possible experimental implementations, we note that there are existing proposals based on cold atoms [63–66] and trapped ions [67]. In these setups, the random on-site potential can be controlled through an auxiliary system using two-body interactions. As a possible future exploration, one could consider quantum control of random interactions [68], which could be realized by a similar disorder mapping together with multibody interactions [69,70], as elaborated in the Appendix.

ACKNOWLEDGMENTS

This work is supported by the National Center for Theoretical Sciences and the National Science and Technology Council, Taiwan, under Grant No. MOST 111-2123-M-006-001.

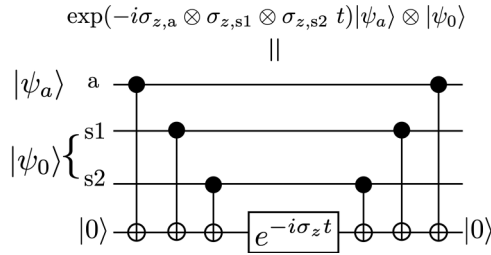


FIG. 6. Circuit implementation of the dynamics governed by the Hamiltonian in Eq. (A2). Here, $|\psi_a\rangle$ and $|\psi_0\rangle$ are the initial states for the ancilla and the system, respectively.

APPENDIX: PHYSICAL REALIZATION OF CONTROLLING RANDOM INTERACTIONS BY QUANTUM ANCILLA

Here, we propose a physical realization for the quantum control of random interactions. It is worth noting that, as already proposed in Ref. [18], quantum control of on-site potentials can be implemented by considering two species of atoms together with two-body interactions between them. For instance, let us consider a two-qubit model, where one qubit represents the system and the other acts as the ancilla. Suppose that the ancilla-system complex is governed by a Hamiltonian

with two-body interaction:

$$\sigma_{z,a} \otimes \sigma_{z,s} = |0_a\rangle\langle 0_a| \otimes \sigma_{z,s} + |1_a\rangle\langle 1_a| \otimes (-\sigma_{z,s}), \quad (\text{A1})$$

where the labels “a” and “s” respectively represent the ancilla and the system qubits. We observe that this two-body interaction enables the mapping of different external fields (+1 and -1) onto the ancilla, thereby allowing quantum control over the potential experienced by the system.

Following a similar approach to the disorder mapping, quantum control over random interactions can be realized by multibody interactions. To illustrate this idea, we consider the simplest scenario, where the interaction of a two-qubit system is controlled by an ancillary qubit. The quantum control is accomplished through the following three-body interaction Hamiltonian:

$$\sigma_{z,a} \otimes \sigma_{z,s1} \otimes \sigma_{z,s2} = |0_a\rangle\langle 0_a| \otimes \sigma_{z,s1} \otimes \sigma_{z,s2} + |1_a\rangle\langle 1_a| \otimes (-\sigma_{z,s1} \otimes \sigma_{z,s2}). \quad (\text{A2})$$

In this case, the ancillary qubit serves as a quantum control for the interactions between system qubits labeled s1 and s2. This multibody interaction can be implemented by analog simulators (such as superconducting circuits [69] or cold atoms [70]) as well as gate-based quantum processors. Specifically, the dynamics governed by Eq. (A2) can be simulated using the circuit model shown in Fig. 6, originally proposed in Ref. [71].

- [1] P. W. Anderson, Absence of diffusion in certain random lattices, *Phys. Rev.* **109**, 1492 (1958).
- [2] R. Nandkishore and D. A. Huse, Many-body localization and thermalization in quantum statistical mechanics, *Annu. Rev. Condens. Matter Phys.* **6**, 15 (2015).
- [3] D. A. Abanin, E. Altman, I. Bloch, and M. Serbyn, Colloquium: Many-body localization, thermalization, and entanglement, *Rev. Mod. Phys.* **91**, 021001 (2019).
- [4] F. Alet and N. Laflorencie, Many-body localization: An introduction and selected topics, *C. R. Phys.* **19**, 498 (2018).
- [5] M. Serbyn, Z. Papić, and D. A. Abanin, Local Conservation Laws and the Structure of the Many-Body Localized States, *Phys. Rev. Lett.* **111**, 127201 (2013).
- [6] D. A. Huse, R. Nandkishore, and V. Oganesyan, Phenomenology of fully many-body-localized systems, *Phys. Rev. B* **90**, 174202 (2014).
- [7] V. Ros, M. Müller, and A. Scardicchio, Integrals of motion in the many-body localized phase, *Nucl. Phys. B* **891**, 420 (2015).
- [8] T. B. Wahl, A. Pal, and S. H. Simon, Efficient Representation of Fully Many-Body Localized Systems Using Tensor Networks, *Phys. Rev. X* **7**, 021018 (2017).
- [9] M. Mierzejewski, M. Kozarzewski, and P. Prelovšek, Counting local integrals of motion in disordered spinless-fermion and Hubbard chains, *Phys. Rev. B* **97**, 064204 (2018).
- [10] S. J. Thomson and M. Schiró, Time evolution of many-body localized systems with the flow equation approach, *Phys. Rev. B* **97**, 060201(R) (2018).
- [11] M. Žnidarič, Entanglement in a dephasing model and many-body localization, *Phys. Rev. B* **97**, 214202 (2018).
- [12] M. Žnidarič, T. Prosen, and P. Prelovšek, Many-body localization in the Heisenberg XXZ magnet in a random field, *Phys. Rev. B* **77**, 064426 (2008).
- [13] J. H. Bardarson, F. Pollmann, and J. E. Moore, Unbounded Growth of Entanglement in Models of Many-Body Localization, *Phys. Rev. Lett.* **109**, 017202 (2012).
- [14] M. Serbyn, Z. Papić, and D. A. Abanin, Universal Slow Growth of Entanglement in Interacting Strongly Disordered Systems, *Phys. Rev. Lett.* **110**, 260601 (2013).
- [15] M. Serbyn, M. Knap, S. Gopalakrishnan, Z. Papić, N. Y. Yao, C. R. Laumann, D. A. Abanin, M. D. Lukin, and E. A. Demler, Interferometric Probes of Many-Body Localization, *Phys. Rev. Lett.* **113**, 147204 (2014).
- [16] M. Serbyn and D. A. Abanin, Loschmidt echo in many-body localized phases, *Phys. Rev. B* **96**, 014202 (2017).
- [17] B. Chiaro *et al.*, Direct measurement of nonlocal interactions in the many-body localized phase, *Phys. Rev. Res.* **4**, 013148 (2022).
- [18] B. Paredes, F. Verstraete, and J. I. Cirac, Exploiting Quantum Parallelism to Simulate Quantum Random Many-Body Systems, *Phys. Rev. Lett.* **95**, 140501 (2005).
- [19] G. A. Álvarez, E. P. Danieli, P. R. Levstein, and H. M. Pastawski, Quantum Parallelism as a Tool for Ensemble Spin Dynamics Calculations, *Phys. Rev. Lett.* **101**, 120503 (2008).
- [20] F. Andraschko, T. Enss, and J. Sirker, Purification and Many-Body Localization in Cold Atomic Gases, *Phys. Rev. Lett.* **113**, 217201 (2014).
- [21] Z. Papić, E. M. Stoudenmire, and D. A. Abanin, Many-body localization in disorder-free systems: The importance of finite-size constraints, *Ann. Phys.* **362**, 714 (2015).

- [22] G. Chiribella and H. Kristjánsson, Quantum Shannon theory with superpositions of trajectories, *Proc. R. Soc., Ser. A* **475**, 20180903 (2019).
- [23] N. Loizeau and A. Grinbaum, Channel capacity enhancement with indefinite causal order, *Phys. Rev. A* **101**, 012340 (2020).
- [24] A. A. Abbott, J. Wechs, D. Horsman, M. Mhalla, and C. Branciard, Communication through coherent control of quantum channels, *Quantum* **4**, 333 (2020).
- [25] H. Kristjánsson, G. Chiribella, S. Salek, D. Ebler, and M. Wilson, Resource theories of communication, *New J. Phys.* **22**, 073014 (2020).
- [26] G. Rubino, L. A. Rozema, D. Ebler, H. Kristjánsson, S. Salek, P. Allard Guérin, A. A. Abbott, C. Branciard, Č. Brukner, G. Chiribella, and P. Walther, Experimental quantum communication enhancement by superposing trajectories, *Phys. Rev. Res.* **3**, 013093 (2021).
- [27] H.-Y. Ku, K.-Y. Lee, P.-R. Lai, J.-D. Lin, and Y.-N. Chen, Coherent activation of a steerability-breaking channel, *Phys. Rev. A* **107**, 042415 (2023).
- [28] G. Rubino, G. Manzano, and Č. Brukner, Quantum superposition of thermodynamic evolutions with opposing time's arrows, *Commun. Phys.* **4**, 251 (2021).
- [29] H. Nie, T. Feng, S. Longden, and V. Vedral, Quantum cooling activated by coherent-controlled thermalisation, [arXiv:2201.06954](https://arxiv.org/abs/2201.06954).
- [30] F.-J. Chan, Y.-T. Huang, J.-D. Lin, H.-Y. Ku, J.-S. Chen, H.-B. Chen, and Y.-N. Chen, Maxwell's two-demon engine under pure dephasing noise, *Phys. Rev. A* **106**, 052201 (2022).
- [31] P.-R. Lai, J.-D. Lin, Y.-T. Huang, and Y.-N. Chen, Quick charging of a quantum battery with superposed trajectories, [arXiv:2307.09010](https://arxiv.org/abs/2307.09010).
- [32] F. Chapeau-Blondeau, Quantum parameter estimation on coherently superposed noisy channels, *Phys. Rev. A* **104**, 032214 (2021).
- [33] K.-Y. Lee, J.-D. Lin, A. Miranowicz, F. Nori, H.-Y. Ku, and Y.-N. Chen, Steering-enhanced quantum metrology using superpositions of noisy phase shifts, *Phys. Rev. Res.* **5**, 013103 (2023).
- [34] O. Siltanen, Breaking the quantum Cramer-Rao bound with non-Markovian memory effects, [arXiv:2211.05142](https://arxiv.org/abs/2211.05142).
- [35] M. Ban, Two-qubit correlation in two independent environments with indefiniteness, *Phys. Lett. A* **385**, 126936 (2021).
- [36] M. Ban, Relaxation process of a two-level system in a coherent superposition of two environments, *Quantum Inf. Process.* **19**, 351 (2020).
- [37] O. Siltanen, T. Kuusela, and J. Piilo, Interferometric approach to open quantum systems and non-Markovian dynamics, *Phys. Rev. A* **103**, 032223 (2021).
- [38] J.-D. Lin, C.-Y. Huang, N. Lambert, G.-Y. Chen, F. Nori, and Y.-N. Chen, Space-time dual quantum Zeno effect: Interferometric engineering of open quantum system dynamics, *Phys. Rev. Res.* **4**, 033143 (2022).
- [39] J. Foo, R. B. Mann, and M. Zych, Entanglement amplification between superposed detectors in flat and curved spacetimes, *Phys. Rev. D* **103**, 065013 (2021).
- [40] J. Foo, S. Onoe, and M. Zych, Unruh-deWitt detectors in quantum superpositions of trajectories, *Phys. Rev. D* **102**, 085013 (2020).
- [41] L. J. Henderson, A. Belenchia, E. Castro-Ruiz, C. Budroni, M. Zych, Č. Brukner, and R. B. Mann, Quantum Temporal Superposition: The Case of Quantum Field Theory, *Phys. Rev. Lett.* **125**, 131602 (2020).
- [42] A. Pal and D. A. Huse, Many-body localization phase transition, *Phys. Rev. B* **82**, 174411 (2010).
- [43] D. J. Luitz, N. Laflorencie, and F. Alet, Many-body localization edge in the random-field Heisenberg chain, *Phys. Rev. B* **91**, 081103(R) (2015).
- [44] M. Schreiber, S. S. Hodgman, P. Bordia, H. P. Lüschen, M. H. Fischer, R. Vosk, E. Altman, U. Schneider, and I. Bloch, Observation of many-body localization of interacting fermions in a quasirandom optical lattice, *Science* **349**, 842 (2015).
- [45] J. Smith, A. Lee, P. Richerme, B. Neyenhuis, P. W. Hess, P. Hauke, M. Heyl, D. A. Huse, and C. Monroe, Many-body localization in a quantum simulator with programmable random disorder, *Nat. Phys.* **12**, 907 (2016).
- [46] J.-y. Choi, S. Hild, J. Zeiher, P. Schauß, A. Rubio-Abadal, T. Yefsah, V. Khemani, D. A. Huse, I. Bloch, and C. Gross, Exploring the many-body localization transition in two dimensions, *Science* **352**, 1547 (2016).
- [47] K. Xu, J.-J. Chen, Y. Zeng, Y.-R. Zhang, C. Song, W. Liu, Q. Guo, P. Zhang, D. Xu, H. Deng, K. Huang, H. Wang, X. Zhu, D. Zheng, and H. Fan, Emulating Many-Body Localization with a Superconducting Quantum Processor, *Phys. Rev. Lett.* **120**, 050507 (2018).
- [48] E. V. H. Doggen, F. Schindler, K. S. Tikhonov, A. D. Mirlin, T. Neupert, D. G. Polyakov, and I. V. Gornyi, Many-body localization and delocalization in large quantum chains, *Phys. Rev. B* **98**, 174202 (2018).
- [49] T. Chanda, P. Sierant, and J. Zakrzewski, Many-body localization transition in large quantum spin chains: The mobility edge, *Phys. Rev. Res.* **2**, 032045(R) (2020).
- [50] R. M. Nandkishore and S. L. Sondhi, Many-Body Localization with Long-Range Interactions, *Phys. Rev. X* **7**, 041021 (2017).
- [51] S. Nag and A. Garg, Many-body localization in the presence of long-range interactions and long-range hopping, *Phys. Rev. B* **99**, 224203 (2019).
- [52] S. R. Koshkaki and M. H. Kolodrubetz, Inverted many-body mobility edge in a central qudit problem, *Phys. Rev. B* **105**, L060303 (2022).
- [53] R.-C. Ge, S. R. Koshkaki, and M. H. Kolodrubetz, Cavity induced many-body localization, [arXiv:2208.06898](https://arxiv.org/abs/2208.06898).
- [54] D. D. Vu, K. Huang, X. Li, and S. Das Sarma, Fermionic Many-Body Localization for Random and Quasiperiodic Systems in the Presence of Short- and Long-Range Interactions, *Phys. Rev. Lett.* **128**, 146601 (2022).
- [55] D. Rossini, G. M. Andolina, and M. Polini, Many-body localized quantum batteries, *Phys. Rev. B* **100**, 115142 (2019).
- [56] H. Wang, H.-C. Yeh, and A. Kamenev, Many-body localization enables iterative quantum optimization, *Nat. Commun.* **13**, 5503 (2022).
- [57] Y. Chen, Universal logarithmic scrambling in many body localization, [arXiv:1608.02765](https://arxiv.org/abs/1608.02765).
- [58] S. Xu, X. Li, Y.-T. Hsu, B. Swingle, and S. Das Sarma, Butterfly effect in interacting Aubry-Andre model: Thermalization, slow scrambling, and many-body localization, *Phys. Rev. Res.* **1**, 032039(R) (2019).

- [59] K. A. Landsman, C. Figgatt, T. Schuster, N. M. Linke, B. Yoshida, N. Y. Yao, and C. Monroe, Verified quantum information scrambling, *Nature (London)* **567**, 61 (2019).
- [60] J.-D. Lin, W.-Y. Lin, H.-Y. Ku, N. Lambert, Y.-N. Chen, and F. Nori, Quantum steering as a witness of quantum scrambling, *Phys. Rev. A* **104**, 022614 (2021).
- [61] N. Bölter and S. Kehrein, Scrambling and many-body localization in the XXZ chain, *Phys. Rev. B* **105**, 104202 (2022).
- [62] J. Zhang, P. W. Hess, A. Kyprianidis, P. Becker, A. Lee, J. Smith, G. Pagano, I.-D. Potirniche, A. C. Potter, A. Vishwanath *et al.*, Observation of a discrete time crystal, *Nature (London)* **543**, 217 (2017).
- [63] B. Horstmann, J. I. Cirac, and T. Roscilde, Dynamics of localization phenomena for hard-core bosons in optical lattices, *Phys. Rev. A* **76**, 043625 (2007).
- [64] K. V. Krutitsky, M. Thorwart, R. Egger, and R. Graham, Ultracold bosons in lattices with binary disorder, *Phys. Rev. A* **77**, 053609 (2008).
- [65] B. Horstmann, S. Dürr, and T. Roscilde, Localization of Cold Atoms in State-Dependent Optical Lattices via a Rabi Pulse, *Phys. Rev. Lett.* **105**, 160402 (2010).
- [66] F. Rose and R. Schmidt, Disorder in order: Localization without randomness in a cold-atom system, *Phys. Rev. A* **105**, 013324 (2022).
- [67] A. Bermudez, M. Martin-Delgado, and D. Porras, The localization of phonons in ion traps with controlled quantum disorder, *New J. Phys.* **12**, 123016 (2010).
- [68] P. Sierant, D. Delande, and J. Zakrzewski, Many-body localization due to random interactions, *Phys. Rev. A* **95**, 021601(R) (2017).
- [69] N. Chancellor, S. Zohren, and P. A. Warburton, Circuit design for multi-body interactions in superconducting quantum annealing systems with applications to a scalable architecture, *npj Quantum Inf.* **3**, 21 (2017).
- [70] A. Goban, R. Hutson, G. Marti, S. Campbell, M. Perlin, P. Julienne, J. D'incao, A. Rey, and J. Ye, Emergence of multi-body interactions in a fermionic lattice clock, *Nature (London)* **563**, 369 (2018).
- [71] M. A. Nielsen and I. L. Chuang, *Quantum Computation and Quantum Information: 10th Anniversary Edition* (Cambridge University, Cambridge, England, 2010).